

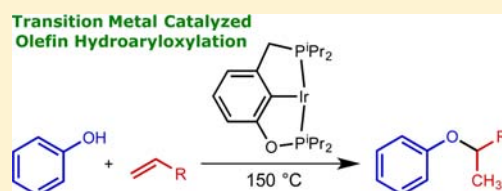
Olefin Hydroaryloxylation Catalyzed by Pincer–Iridium Complexes

Michael C. Haibach, Changjian Guan, David Y. Wang, Bo Li, Nicholas Lease, Andrew M. Steffens, Karsten Krogh-Jespersen,* and Alan S. Goldman*

Department of Chemistry and Chemical Biology, Rutgers, The State University of New Jersey, New Brunswick, New Jersey 08903, United States

S Supporting Information

ABSTRACT: Aryl alkyl ethers, which are widely used throughout the chemical industry, are typically produced via the Williamson ether synthesis. Olefin hydroaryloxylation potentially offers a much more atom-economical alternative. Known acidic catalysts for hydroaryloxylation, however, afford very poor selectivity. We report the organometallic-catalyzed intermolecular hydroaryloxylation of unactivated olefins by iridium “pincer” complexes. These catalysts do not operate via the hidden Brønsted acid pathway common to previously developed transition-metal-based catalysts. The reaction is proposed to proceed via olefin insertion into an iridium–alkoxide bond, followed by rate-determining C–H reductive elimination to yield the ether product. The reaction is highly chemo- and regioselective and offers a new approach to the atom-economical synthesis of industrially important ethers and, potentially, a wide range of other oxygenates.

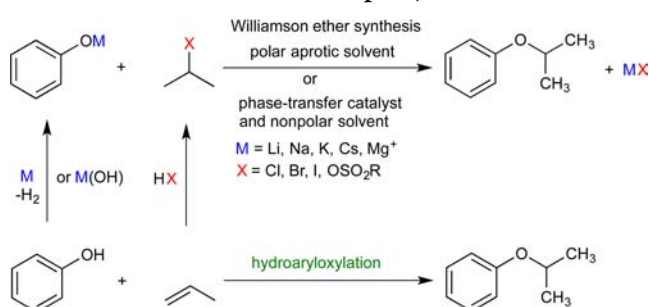


INTRODUCTION

The addition of H–X bonds across olefinic double bonds catalyzed by transition-metal complexes represents a reaction class of great importance in organic chemical synthesis.^{1–3} Recent years have seen significant developments in catalytic hydroamination;^{4–6} however, progress toward the development of transition-metal complexes for catalytic addition of O–H bonds to olefins has been much more limited.^{1–3,6,7} Such additions of alcohol O–H bonds, especially intermolecular, remain a particularly important and attractive challenge.

Alkyl aryl ethers are an important class of commodity chemicals, with applications ranging from solvents to fragrances to pharmaceutical building blocks.⁸ They are currently synthesized primarily via the very classical⁹ Williamson ether synthesis, whereby an alkali salt of the appropriate phenol (performed or generated in situ) is coupled with an alkyl halide or alkyl sulfonate ester, typically in a polar aprotic solvent (Scheme 1).

Scheme 1. Alternative Syntheses of Alkyl Aryl Ethers (Shown for the Addition of Phenol to Propene)



In some cases, phase transfer catalysis can be used to avoid the requirement of a polar aprotic solvent. The use of alkyl alcohols in place of alkyl halides typically requires a gas-phase reaction or dehydrating agent. For the industrially preferred route, 1 equiv of alkali halide or alkali sulfonate waste is generated per equivalent of product produced, in addition to the waste associated with preparation of the alkali phenoxide and the alkyl halide, which is typically prepared from the corresponding olefin.

Despite these drawbacks, the Williamson ether synthesis is widely used for both industrial and small-scale applications, rather than the atom-economical olefin hydroaryloxylation route shown in Scheme 1. This is due at least in part to the fact that, until quite recently, the known catalysts for olefin hydroaryloxylation were all strong Brønsted or Lewis acids such as H₂SO₄ and BF₃·OEt₂. While this class of catalysts is highly active, its use suffers from competing Friedel–Crafts alkylations and very poor chemoselectivity. For example, the reaction of propene with phenol catalyzed by BF₃·OEt₂ affords comparable amounts of both C- and O-isopropylphenol, even at 0 °C.¹⁰ Beginning with He’s report in 2005,¹¹ significant attention has been focused on transition-metal precatalysts for hydroaryloxylation, such as (PPh₃)Au(OTf). Despite early evidence that triflic acid was the catalytically active species,^{12,13} researchers continued to identify numerous transition metal “precatalysts” that were later shown by Hintermann to be Brønsted acid delivery systems (with Ag(OTf) in chlorinated solvents serving as the most common source).^{14,15} Many recent and classic examples employing Lewis acid catalysts, particularly lanthanide triflates, are also proposed to operate via Yamamoto’s Lewis-assisted Brønsted acid¹⁶ mode of activation.^{12,14,15} Indeed, to our knowledge, at the outset of this work there were no well-defined examples of intermolecular

Received: May 7, 2013

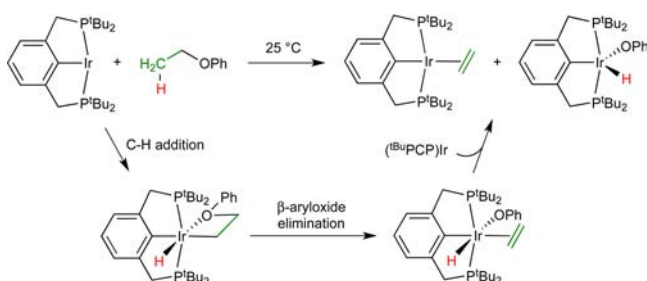
Published: September 12, 2013

addition of alcohol O–H bonds across the double bond of simple olefins directly catalyzed by a transition-metal complex.^{7,14,17} In this communication, we report the first such catalysts, specifically for the reaction of phenols, and support for a likely mechanism on the basis of experimental and computational evidence.¹⁸ These catalysts offer selectivity much greater than, and in some cases orthogonal to, that of previously reported acid catalysts.

RESULTS AND DISCUSSION

We have previously reported that precursors of the fragment $(t^{\text{Bu}}\text{PCP})\text{Ir}(\text{R}^{\text{PCP}})$ ($\text{R}^{\text{PCP}} = \kappa^3\text{-C}_6\text{H}_3\text{-2,6-(CH}_2\text{PR}_2)_2$) could cleave aryl- sp^3 C–O bonds stoichiometrically via an initial C–H oxidative addition step.^{19,20} In the case of ethyl phenyl ether, for example, this led to dehydroaryloxylation and formation of the iridium adducts of ethylene and phenol (Scheme 2). The potential ability

Scheme 2. Stoichiometric Dehydroaryloxylation of Ethyl Phenyl Ether by $(t^{\text{Bu}}\text{PCP})\text{Ir}$



of such species to undergo kinetically facile olefin loss and phenol elimination suggested the possibility of a catalytic cycle; in the thermodynamically favorable reverse direction such a cycle would constitute olefin hydroaryloxylation.

Attempts to effect catalytic hydroaryloxylation by $(t^{\text{Bu}}\text{PCP})\text{Ir}$ (10 mM $(t^{\text{Bu}}\text{PCP})\text{IrH}_4$ catalyst precursor, 500 mM phenol, 1 atm of ethylene or propene, *p*-xylene solvent, 100–150 °C) were unsuccessful, yielding no new organic products. Investigation of some previously reported derivatives of $(t^{\text{Bu}}\text{PCP})\text{Ir}$, however, successfully identified several catalysts active for the addition of propene to 3,5-dimethylphenol at 150 °C (Figure 1).²¹ The three most active derivatives identified were $(t^{\text{Bu}}\text{MePCP})\text{Ir}$,²² $(\text{MeO-}i^{\text{Pr}}\text{PCP})\text{Ir}$,²³ and $(i^{\text{Pr}}\text{PCOP})\text{Ir}$.²⁴

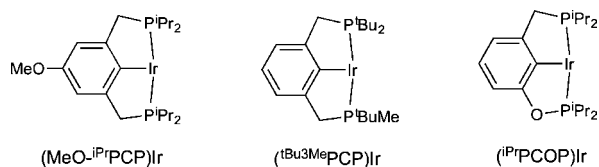
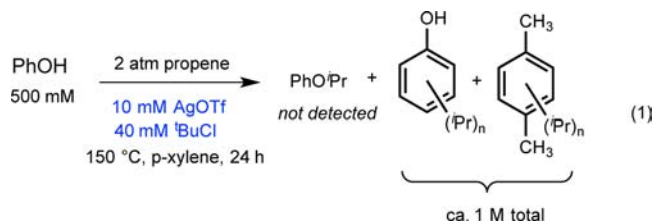


Figure 1. Species found to be active for catalytic hydroaryloxylation.

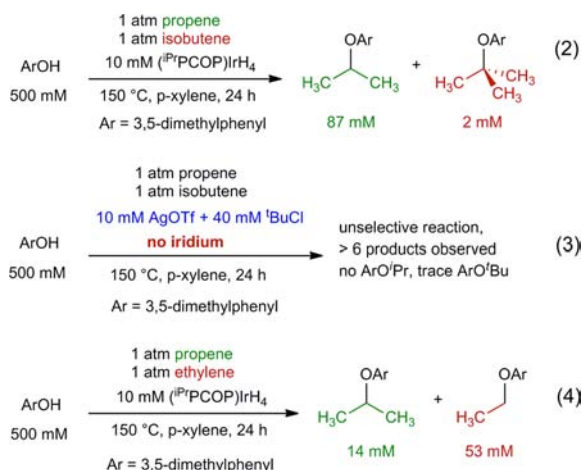
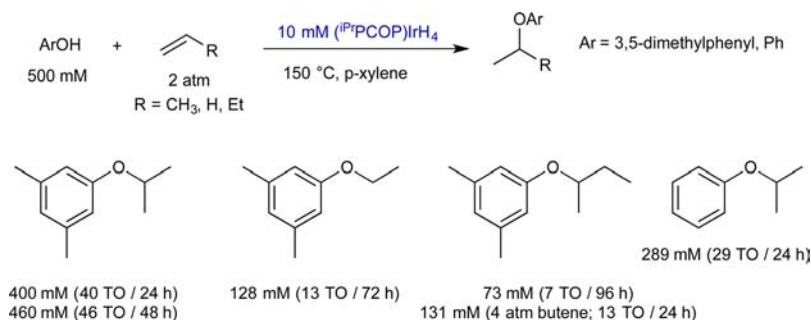
This group of sterically less congested catalysts is about 1 order of magnitude more active for alkane dehydrogenation than $(t^{\text{Bu}}\text{PCP})\text{Ir}$.^{25,26} As in alkane dehydrogenation, the catalytically active species can be generated from the iridium tetrahydride or ethylene complexes under the reaction conditions or from the corresponding (pincer)IrHCl complex and a base.²⁷ Presumably due to inhibition resulting from strong binding by ethylene, the catalytic activity for each (pincer)Ir precatalyst followed the trend $(\text{pincer})\text{Ir}(\text{C}_2\text{H}_4) < (\text{pincer})\text{IrH}_4 \approx (\text{pincer})\text{Ir}(\text{H})(\text{Cl})/\text{NaO}^t\text{Bu}$.

In a typical experiment, *p*-xylene solutions (100 μL) of 10 mM $(i^{\text{Pr}}\text{PCOP})\text{IrH}_4$ ²⁸ and 500 mM 3,5-dimethylphenol are heated at 150 °C in glass ampules sealed with 2 atm of propene. (Each ampule has a total volume of 1.2 mL which holds 1.8 equiv of propene in the gas phase per equivalent of alcohol, plus any propene which may have dissolved in solution prior to sealing.) After 24 h the appearance of 400 mM isopropyl aryl ether (40 catalytic turnovers (TO)) was observed (by GC), while in another ampule 460 mM was observed after 48 h (Scheme 3). No *n*-propyl aryl ether or other alkylphenols were detectable by GC, indicating that the reaction is fully regio- and chemoselective. The analogous reaction with ethylene yields exclusively ethyl aryl ether (47 mM after 24 h, 128 mM after 72 h). 1-Butene also yields only the iso product, albeit with lower conversion than either ethylene or propene (Scheme 3). Running the same reaction at 4 atm of 1-butene affords higher conversion. Importantly, when (unsubstituted) phenol and propene are allowed to react, only isopropyl phenyl ether (289 mM) is observed after 24 h. Note that any catalyst operating by the “hidden Brønsted acid” mechanism proposed by Hintermann is expected to afford at least some C-alkylphenol. Indeed, the reaction of phenol and propene using 10 mM Hintermann’s Brønsted acid catalyst (10 mM AgOTf and 40 mM $t^{\text{Bu}}\text{Cl}$)¹⁵ yields no isopropyl phenyl ether after 24 h. Instead, 10 different products are observable by GC, with both phenol and the *p*-xylene solvent undergoing apparently unselective Friedel–Crafts alkylations and isomerizations (eq 1).



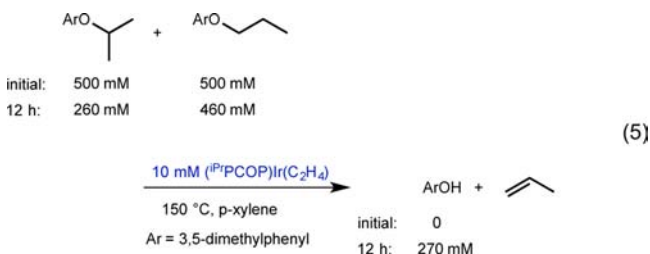
Further evidence of the nonacidic nature of the iridium catalyst system derives from a competition experiment between isobutene and propene. Isobutene forms a much more stable carbocation when protonated; hence, an acidic catalyst would be expected to yield the *tert*-butyl phenyl ether as the major product. However, when a solution of 3,5-dimethylphenol and $(i^{\text{Pr}}\text{PCOP})\text{IrH}_4$ is subjected to equal partial pressures of isobutene and propene, the aryl isopropyl ether is formed with >40:1 selectivity (eq 2). The control experiment, using AgOTf/*t*-BuCl, gave no aryl isopropyl ether, although only trace aryl *tert*-butyl ether was observed (eq 3); the major products resulted from Friedel–Crafts alkylation of the arene rings as in the case of eq 1. Similarly arguing against any carbocation-derived selectivity, although propene reacts significantly faster with 3,5-dimethylphenol than does ethylene in independent experiments, ethylene reacts preferentially vs propene with selectivity >3:1 in an internal competition experiment (eq 4).

The apparently high regioselectivity for formation of *i*-PrOAr vs *n*-PrOAr (Scheme 3) and the high chemoselectivity for hydroaryloxylation of propene vs isobutene (eq 2) might be attributed, a priori, to thermodynamic rather than kinetic factors. In such a case the rate of the respective hydroaryloxylation might be comparable to or even more rapid than the reaction to give *i*-PrOAr, but the respective dehydroaryloxylation back-reactions could be even faster. To test this hypothesis, we investigated the possible back reactions.

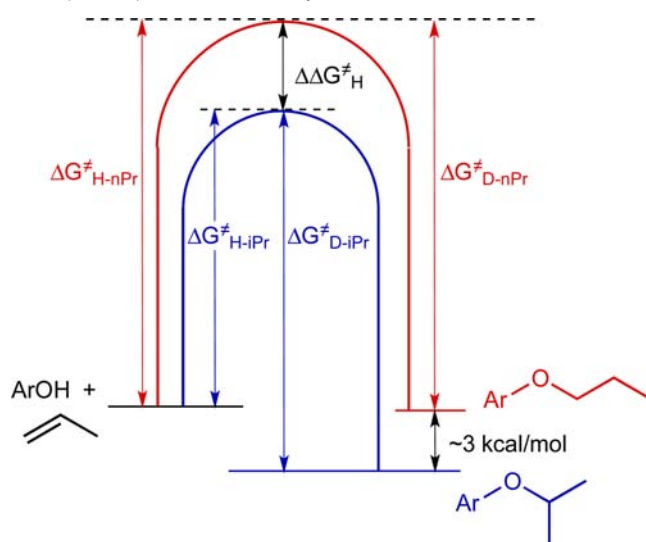
Scheme 3. Hydroaryloxylation of Olefins Catalyzed by $(i\text{PrPCOP})\text{IrH}_4$ 

A *p*-xylene solution of *i*-PrOAr (500 mM), *n*-PrOAr (500 mM), and $(i\text{PrPCOP})\text{Ir}(\text{C}_2\text{H}_4)$ was sealed under vacuum (100 μL in a 1 mL ampule) and heated to 150 °C. After 12 h, GC analysis revealed the disappearance of 48% of the *i*-PrOAr and 8% of the *n*-PrOAr, with commensurate appearance of ArOH (270 mM) and the appearance of propene.²⁹ Thus, the rates of both propene hydroaryloxylation to give *n*-PrOAr and the dehydroaryloxylation of *n*-PrOAr are much slower than the corresponding reactions for *i*-PrOAr; this selectivity is therefore clearly a kinetic phenomenon.

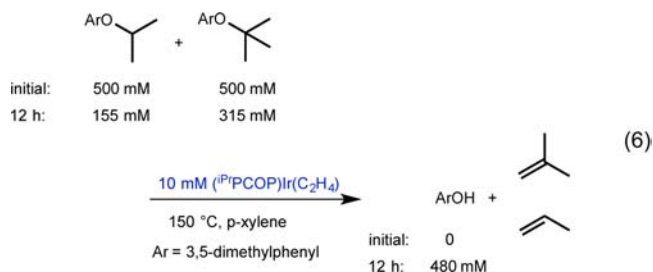
Note that the dehydroaryloxylation of *i*-PrOAr proceeds at least 6-fold more rapidly than that of *n*-PrOAr (eq 5). Both



experimental data³⁰ and DFT calculations (discussed below) indicate that the free energy of *n*-PrOAr is ca. 3 kcal/mol higher than that of *i*-PrOAr. $\Delta\Delta G_{\text{H}}^\ddagger$ for the hydroaryloxylation of propene to give *n*-PrOAr must therefore be ca. 3 kcal/mol greater than $\Delta\Delta G_{\text{D}}^\ddagger$ for the dehydroaryloxylation (Scheme 4). In that case, a 6-fold rate difference for the latter, at 150 °C, would correspond to a rate difference of $6 \exp(-3 \text{ kcal/mol}/(RT)) \approx 200$ (i.e., $\Delta\Delta G_{\text{H}}^\ddagger \approx 4.5 \text{ kcal/mol}$), in accord with our conclusion of essentially complete kinetic selectivity for the formation of *i*-PrOAr in the hydroaryloxylation.

Scheme 4. Schematic Free Energy Profile for Hydroaryloxylation of Propene To Give *i*-PrOAr and *n*-PrOAr and the Corresponding Dehydroaryloxylation Catalyzed by $(i\text{PrPCOP})\text{IrH}_4$ at 150 °C

A competition experiment under the same conditions as for the experiment of eq 5 was also conducted with *i*-PrOAr and *t*-BuOAr. The dehydroaryloxylation of *i*-PrOAr was found to be more rapid (by a factor larger than 2; eq 6). Thus, the much greater rate of hydroaryloxylation of propene vs isobutene (>40-fold; eq 2), like the regioselectivity to give *i*-PrOAr, is a kinetic phenomenon.

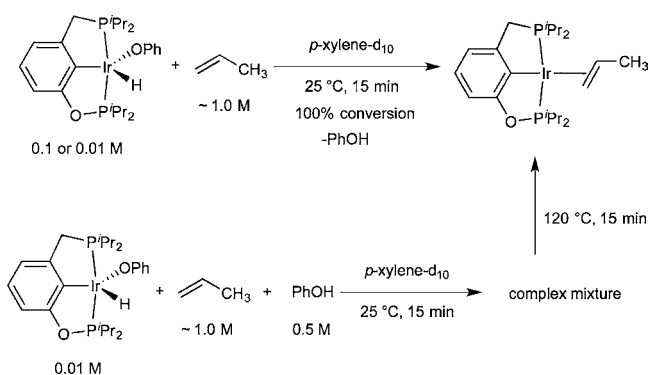


Finally, we note that, even in the presence of a large excess of NaO^tBu (125 mM), a solution of 3,5-dimethylphenol (0.5 M) under propene (2 atm) undergoes clean catalytic hydroaryloxylation by $(i\text{Bu}^3\text{MePCP})\text{IrHCl}$ (10 mM), yielding 250 mM *i*-PrOAr product after 24 h at 150 °C. This result argues strongly against any mechanism involving Brønsted acid.

Identification of the Catalyst Resting State. The reaction of phenol with propene using $(i\text{PrPCOP})\text{Ir}$ as the catalyst was

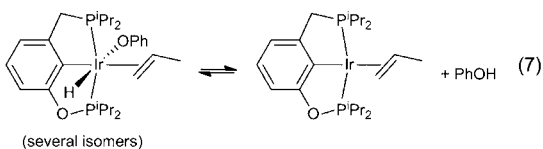
investigated in detail by ^1H and ^{31}P NMR. Addition of 1 atm of propene to a J. Young NMR tube with either a 0.1 or 0.01 M solution of $(^{\text{iPr}}\text{PCOP})\text{Ir}(\text{H})(\text{OPh})^{19}$ in *p*-xylene- d_{10} (affording a solution propene concentration of ca. 1 M) results in quantitative conversion to the $(^{\text{iPr}}\text{PCOP})\text{Ir}(\eta^2\text{-propene})$ complex (see the Supporting Information for characterization of $(^{\text{iPr}}\text{PCOP})\text{Ir}(\eta^2\text{-propene})$ and $(^{\text{iPr}}\text{PCOP})\text{Ir}(\text{H})(\text{OPh})$ and free phenol within 15 min at 25 °C (Scheme 5). No change is observed upon heating to

Scheme 5. Identification of $(^{\text{iPr}}\text{PCOP})\text{Ir}(\eta^2\text{-propene})$ as the Catalyst Resting State by NMR Studies



120 °C in the NMR spectrometer. Importantly, no signals between δ 0 and -50 ppm in the ^1H NMR spectrum, characteristic of iridium hydrides, are observed, thus indicating the lack of formation of any appreciable amounts of either $(^{\text{iPr}}\text{PCOP})\text{Ir}(\eta^2\text{-propene})(\text{H})(\text{OPh})$ or $(^{\text{iPr}}\text{PCOP})\text{Ir}[\text{CH}_2\text{CH}(\text{OAr})\text{CH}_3](\text{H})$ under these conditions.

A solution otherwise similar to that described above was prepared, but with 0.5 M PhOH added (0.01 M $(^{\text{iPr}}\text{PCOP})\text{Ir}(\text{H})(\text{OPh})$, 0.5 M PhOH, ca. 1 M propene) to replicate the concentrations typically used for the catalytic runs. Under these conditions, the presence of PhOH resulted in a complex mixture of iridium-containing complexes at 25 °C (^{31}P and ^1H NMR). $(^{\text{iPr}}\text{PCOP})\text{Ir}(\eta^2\text{-propene})$ is present, while several signals between δ -7 and -24 ppm (triplets with J values of ca. 15 Hz which is typical for $^2J_{\text{PH}}$) are also observed in the ^1H NMR spectrum. These signals are indicative of six-coordinate iridium hydrides; it would seem likely that at least some of these are of the composition $(^{\text{iPr}}\text{PCOP})\text{Ir}(\eta^2\text{-propene})(\text{OPh})(\text{H})$. The low symmetry of these complexes, however, apparently generates several isomers, making assignment of their structures by NMR prohibitively difficult. (Note that even a single coordination isomer of $(^{\text{iPr}}\text{PCOP})\text{Ir}(\eta^2\text{-propene})(\text{OPh})(\text{H})$ has at least four possible conformers depending upon the orientation of the propene ligand.) When this solution is heated to 120 °C, 31 however, a temperature at which there is catalytic activity, the only species observable in solution is $(^{\text{iPr}}\text{PCOP})\text{Ir}(\eta^2\text{-propene})$. Thus, the apparent equilibrium of $(^{\text{iPr}}\text{PCOP})\text{Ir}(\eta^2\text{-propene})(\text{OPh})(\text{H})$ isomers with $(^{\text{iPr}}\text{PCOP})\text{Ir}(\eta^2\text{-propene})$ plus free phenol (eq 7) is driven toward the side with free phenol at higher temperature (as would be expected), and $(^{\text{iPr}}\text{PCOP})\text{Ir}(\eta^2\text{-propene})$ is the resting state under catalytic conditions.



Computational Investigation of the Mechanism.

Computational (DFT 21) studies have been conducted which shed light on the mechanism and selectivity of the hydroaryloxylation reactions. We employed the widely used M06 and M06-L density functionals. Both functionals predicted regio- and chemoselectivity in full agreement with our experimental results. Since the M06-L functional provided slightly better quantitative agreement, we will primarily discuss M06-L energies and present those values in the figures shown here; energies obtained with the M06 functional are given in tables in the Supporting Information. We have focused on the reaction of phenol with propene by our most effective catalyst, $(^{\text{iPr}}\text{PCOP})\text{Ir}$. Although the calculations assume idealized gas-phase conditions, free energies have been calculated at conditions (T , P) that are closer to those of the actual catalytic experiments than are standard conditions ($T = 298.15$ K, $P = 1.0$ atm). Specifically, we use $T = 150$ °C = 423.15 K and, in order to approximate the concentrations of reagents in solution, partial pressures of 34.7 atm were assumed, which correspond to concentrations of 1 mol/L at 150 °C.

Experimentally, as noted above, $(^{\text{iPr}}\text{PCOP})\text{Ir}(\eta^2\text{-propene})$ (**1a**) was found to be the only major species in solution under the standard reaction conditions. Using the M06 functional and the thermodynamic conditions noted above ($T = 150$ °C, $P = 34.7$ atm), $(^{\text{iPr}}\text{PCOP})\text{Ir}(\eta^2\text{-propene})$ was indeed computed to be the lowest energy species, 1.7 kcal/mol lower in free energy than $(^{\text{iPr}}\text{PCOP})\text{Ir}(\text{H})(\text{OPh})$ (**3**) (Table S4, Supporting Information) and 3.9 kcal/mol below $(^{\text{iPr}}\text{PCOP})\text{Ir}(\text{H})(\eta^2\text{-propene})(\text{OPh})$ (**4**) (the lowest energy conformer, with propene coordinated trans to the pincer aryl group; Table S5, Supporting Information). The corresponding M06-L values for $(^{\text{iPr}}\text{PCOP})\text{Ir}(\text{H})(\text{OPh})$ and $(^{\text{iPr}}\text{PCOP})\text{Ir}(\text{H})(\eta^2\text{-propene})(\text{OPh})$, relative to **1a**, are -2.3 and -0.1 kcal/mol at 150 °C, respectively (Table S1, Supporting Information). In both cases, we judge the differences to be within the error margins of the calculations when comparing species that are significantly different (e.g., an Ir(I) complex and an Ir(III) complex, π vs σ coordination, 4-coordination vs 5- or 6-coordination). Accordingly, we will only consider energies relative to the experimentally observed resting state, the olefin π -complex **1a**.

Under typical reaction conditions, $(^{\text{iPr}}\text{PCOP})\text{Ir}(\eta^2\text{-propene})$ (**1a**) is calculated to be the major resting state (the kinetically accessible species of lowest free energy) in the $(^{\text{iPr}}\text{PCOP})\text{Ir}/\text{phenol}/\text{propene}$ system using the M06 functional. However, at 25 °C the free energy of $(^{\text{iPr}}\text{PCOP})\text{Ir}(\text{H})(\eta^2\text{-propene})(\text{OPh})$ is calculated to be -0.6 kcal/mol below the four-coordinate propene adduct, whereas $(^{\text{iPr}}\text{PCOP})\text{Ir}(\text{H})(\text{OPh})$ remains higher in energy than **1a** by 2.0 kcal/mol. The corresponding M06-L values for $(^{\text{iPr}}\text{PCOP})\text{Ir}(\text{H})(\text{OPh})$ and $(^{\text{iPr}}\text{PCOP})\text{Ir}(\text{H})(\eta^2\text{-propene})(\text{OPh})$, relative to **1a**, are -2.1 and -4.5 kcal/mol at 25 °C. These results are consistent (at least within the limits of precision of the calculations) with the observation that a mixture of $(^{\text{iPr}}\text{PCOP})\text{Ir}(\eta^2\text{-propene})$, $(^{\text{iPr}}\text{PCOP})\text{Ir}(\text{H})(\text{OPh})$, and $(^{\text{iPr}}\text{PCOP})\text{Ir}(\text{H})(\eta^2\text{-propene})(\text{OPh})$ appear to be present in a typical reaction solution at 25 °C, whereas only $(^{\text{iPr}}\text{PCOP})\text{Ir}(\eta^2\text{-propene})$ is observed at 120 °C.

The results of the selectivity experiments discussed above argue strongly against a Brønsted-acid catalyzed pathway, or any pathway involving a carbocationic or carbocation-like intermediate, and instead favor a genuinely “organometallic-catalyzed” mechanism. Generally speaking, “organometallic” mechanisms for hydrofunctionalization (addition of species H–X across multiple bonds) may proceed via insertion of olefin into a M–H bond followed by alkyl–X elimination (Figure 2a);

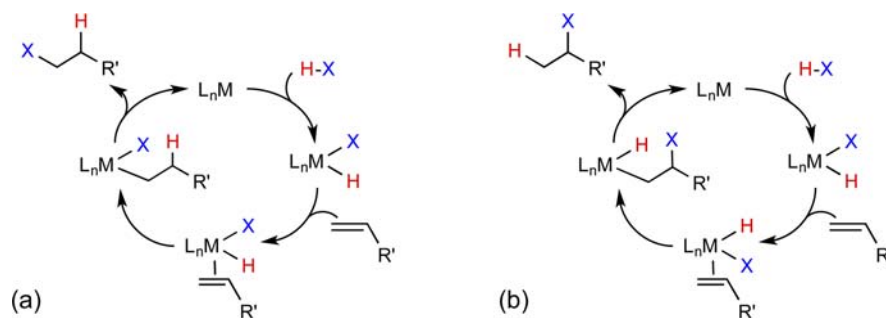


Figure 2. Typical “organometallic” pathways (proceeding via H–X addition, olefin insertion, and C–X or C–H elimination) for generic hydrofunctionalization of an olefin (addition of H–X). Cycle a is shown giving anti-Markovnikov product, and cycle b is shown giving the Markovnikov product. This represents the regioselectivity commonly expected of each pathway, but neither mechanism is necessarily limited to either type of regioselectivity.

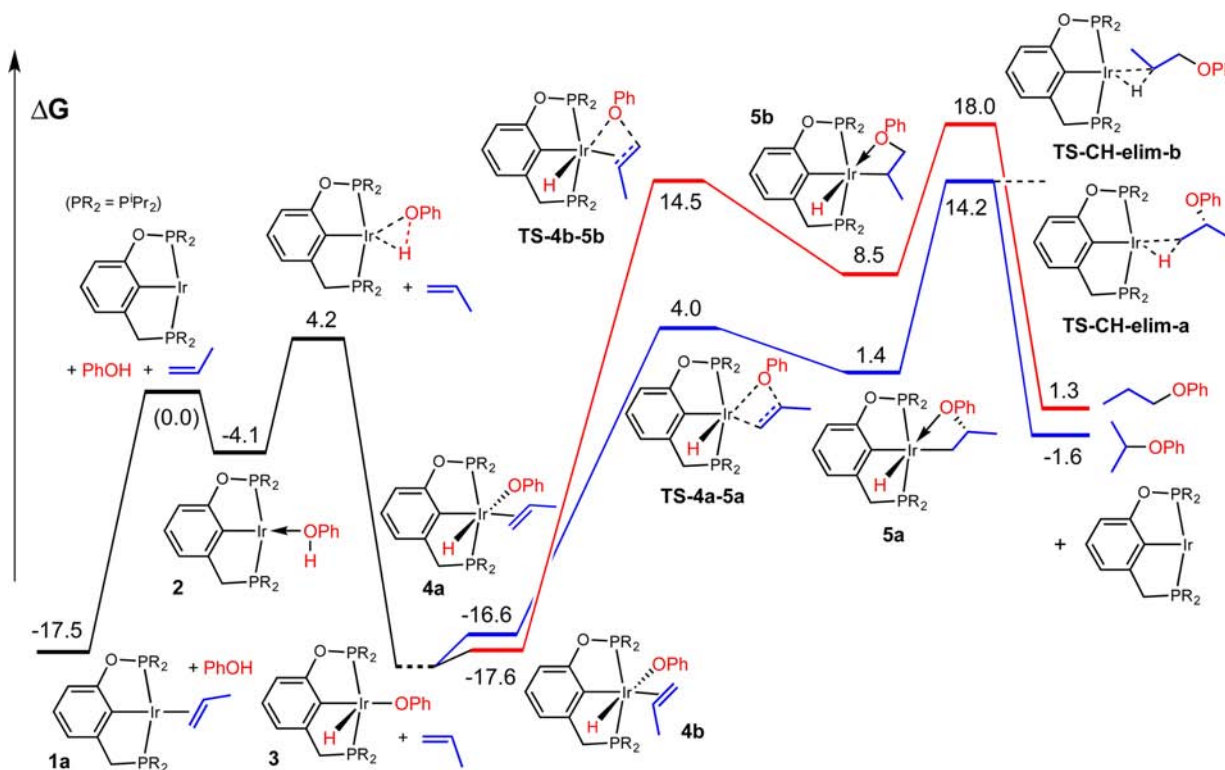


Figure 3. Free energy diagram (M06-L; values of ΔG in kcal/mol) for the proposed 1,2-Ir–O addition pathway for hydrophenoxylation of propene by $(iPrPCOP)Ir$ to give *i*-ProAr (observed product; blue lines) and *n*-ProAr (not observed; red lines).

known examples include $X = SiR_3, BR_2, CN$.¹ Such mechanisms can favor formation of anti-Markovnikov products (e.g., CH_2X-CH_2R from $CH_2=CHR$ plus HX). It is generally assumed that such selectivity is attributable to the preference of transition metals for less substituted alkyl ligands^{32–35} (e.g., primary vs secondary) reflected in the TS preceding or perhaps following the intermediate species $L_nM(alkyl)X$.

In the case of the present system, the free energy calculated for the TS for the key step of C–X elimination as per Figure 2a ($L_nM = (iPrPCOP)Ir$; $X = OPh$; alkyl = *i*-Pr) is 47.3 kcal/mol above that of the calculated resting state, $(iPrPCOP)Ir(propene)$ (M06-L; Table S1, Supporting Information). This value is substantially greater than the overall barrier indicated by experiment, $\Delta G^\ddagger \approx 32$ kcal/mol (based on ca. 1.2 turnovers/h). The pathway of Figure 2a is thus calculated not to be viable in this case, regardless of the energies of any other intermediates and transition states in that pathway. This result is consistent with and closely related to

our previous work, in which it was found that the barrier to direct C–O bond oxidative addition to $(tBuPCP)Ir$ is prohibitively high.^{19,20}

Interestingly, although the pathway of Figure 2a is precluded by the high barrier to C–O bond elimination, the initial steps appear to be quite favorable. Addition of ArOD (0.5 M) and (perpropio) propene (1 atm) to a *p*-xylene- d_{10} solution of $(iPrPCOP)IrH_4$, to give the mixture of species indicated in eq 6 (and isotopologues thereof), results in rapid H/D exchange between propene and ArOD (50% conversion to ArOH within 15 min at room temperature, as revealed in the 1H NMR spectrum). This is most easily explained in terms of reversible insertion of propene into the Ir–H/D bond of $(iPrPCOP)Ir(\eta^2-propene)(OPh)(H/D)$. The thermodynamics of this insertion are calculated to be quite allowable for such an exchange mechanism ($\Delta G = +7.3$ and $+8.6$ kcal/mol for 1,2- and 2,1-Ir–H

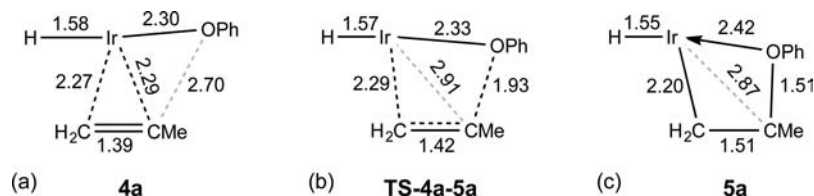


Figure 4. Calculated distances (Å) for the H–Ir–C–C(propene)–O(phenoxide) unit for the 1,2–Ir–O insertion step: (a) *trans*-(^{iPr}PCOP)IrH(OPh)(propene) (**4a**); (b) TS for propene insertion (**TS-4a-5a**); (c) insertion product (^{iPr}PCOP)IrH[CH₂CH(CH₃)OPh] (**5a**).

addition, respectively), although we have been unable to locate appropriate low-energy TS's for these insertions.

Rather than the mechanism indicated in Figure 2a, the calculations are instead consistent with the hypothesis that led to this work: namely, that the mechanism indicated in Scheme 2 could be implemented catalytically in the reverse direction (as shown explicitly in Figure 2b). The mechanism of Figure 2b proceeds via olefin insertion into the M–X (Ir–O) bond, rather than insertion into the M–H bond as in Figure 2a, and is followed by C–H rather than C–X (C–O) elimination. There are relatively few well-characterized examples of insertion of olefins into transition metal–oxygen bonds, but the reaction is certainly not without precedent.^{36–40}

Figure 3 shows the results of calculations of the catalytic cycle (as per Figure 2b) for the (^{iPr}PCOP)Ir-catalyzed reaction of propene and phenol to give *i*-PrOPh and *n*-PrOPh (all free energies are expressed relative to the free three-coordinate pincer iridium complex and free propene and phenol). 1,2-Addition of the Ir–OPh bond of (^{iPr}PCOP)IrH(OPh)(η^2 -propene) (**4a**) across the double bond of coordinated propene is calculated to have a barrier of only ca. 21 kcal/mol, with a transition state (TS; **TS-4a-5a**) that is 21.5 kcal/mol above the propene complex resting state (**1a**). This is in agreement with a theoretical study³⁹ by Hartwig on olefin insertion into the Rh–X bond (X = CH₃, NH₂, OH) of (PMe₃)₂RhX, in which it was calculated that the barrier to 1,2-insertion of coordinated propene into a Rh–O bond was 19.3 kcal/mol. Moreover, also in accord with Hartwig's results,³⁹ in the present system the metal–oxygen bond remains largely intact during and even after the insertion step. The Ir–O bond distances in *trans*-(^{iPr}PCOP)IrH(OPh)(propene) (**4a**), **TS-4a-5a**, and the insertion product **5a** are 2.30, 2.33, and 2.42 Å, respectively (Figure 4); thus, the Ir–O bond appears to transition smoothly from formally covalent to dative.³⁹ A conformer of **5a** in which there is no significant Ir–O interaction ($d_{\text{Ir-O}} = 4.4$ Å) is a local minimum with a free energy 7.0 kcal/mol above the lowest free energy conformer of **5a**; this value presumably represents the approximate strength of the dative interaction.

The product of the 1,2–Ir–OPh addition to propene, (^{iPr}PCOP)Ir[CH₂CH(OPh)CH₃](H) (**5a**), is 18.9 kcal/mol above the propene resting state **1a** (Figure 3). The TS for C–H elimination from this species (**TS-CH-elim-a**), to give *i*-PrOPh, is calculated to have a free energy 31.7 kcal/mol above the resting state (i.e., 14.2 kcal/mol above the reference); this TS leads to a C–H σ -bond complex (not shown in Figure 3) that is 22.9 kcal/mol above the resting state (i.e., 5.4 kcal/mol above the reference). We have been unable to locate a proper TS for dissociation of this σ -bond complex. However, it seems likely (although not certain) that loss of the σ -C–H-bond ether product (which may proceed dissociatively or via displacement by solvent, phenol, or propene) is fast relative to the back reaction, C–H addition. In that case, the C–H elimination is the rate-determining step for formation of *i*-PrOPh, with an overall

calculated barrier height of 31.7 kcal/mol (**TS-CH-elim-a**), in complete (and presumably fortuitously excellent) agreement with the approximate experimental barrier, $\Delta G^\ddagger \approx 32$ kcal/mol.

Figure 3 also shows a pathway that proceeds via a 2,1–Ir–O addition which would lead to *n*-PrOPh; this represents the mechanism shown in Figure 2b but with the reverse regioselectivity. The 2,1–Ir–O addition has a calculated barrier substantially higher than the 1,2–Ir–O addition; **TS-4b-5b** is 32.0 kcal/mol above the resting state vs 21.5 kcal/mol for **TS-4a-5a**. The energy of the resulting phenoxy-substituted secondary alkyl hydride, **5b**, is 7.1 kcal/mol above that of the primary alkyl hydride, **5a**, derived from the 1,2-addition (26.0 kcal/mol above the resting state vs 18.9 kcal/mol). This is also in agreement with Hartwig's study, in which it was found that 1,2-addition of the M–O bond was much more favorable than 2,1-addition (with the difference being much greater than that found for M–C addition).³⁹ However, while these 1,2–Ir–O addition energies are higher than the corresponding values for the 2,1–Ir–O addition, they are not so high as to necessarily preclude formation of the *n*-propyl ether at a rate comparable to that observed for formation of *i*-PrOAr.

The calculations illustrated in Figure 3 predict that the subsequent C–H elimination, not insertion into the Ir–OAr bond, is both rate and product determining. The TS for the C–H elimination, **TS-CH-elim-b**, is of higher energy for the secondary alkyl hydride than for the primary, **TS-CH-elim-a**, by a substantial margin of 3.8 kcal/mol. This difference would correspond to a factor of greater than 90 in the rates for formation of *i*-PrOAr ($\Delta G^\ddagger_{\text{calc}} = 31.7$ kcal/mol) vs *n*-PrOAr ($\Delta G^\ddagger_{\text{calc}} = 35.5$ kcal/mol) at 150 °C. The calculations thus fully account for the observed rate of formation of *i*-PrOAr and for the absence of *n*-PrOAr. Moreover, the same energy diagram illustrates that the barrier to the back reaction (dehydroaryloxylation) is calculated to be slightly higher for the reaction of *i*-PrOPh than for *n*-PrOPh (by 0.9 kcal/mol). This is also in excellent agreement with experimental observations noted above.

The free energy difference between the two rate-determining C–H elimination TS's, which may determine the very high regioselectivity for formation of *i*-PrOAr vs *n*-PrOAr, can perhaps be most simply explained by considering the reaction proceeding in the *reverse* direction. The difference of 3.8 kcal/mol can then be viewed as resulting from a combination of two simple factors (i) The energy of free *i*-PrOAr is lower than that of free *n*-PrOAr (2.9 kcal/mol calculated difference, 3.35 ± 0.43 kcal/mol experimental³⁰). (ii) The barrier for the oxidative cleavage of primary C–H bonds is generally less than for secondary C–H bonds;³⁴ in this case addition of the primary C–H bond of *i*-PrOPh is calculated to be 0.9 kcal/mol lower than that for the secondary C–H (C2) bond of *n*-PrOPh.

Overall, the calculated results presented above, obtained with the use of the M06-L functional, strongly indicate that C–H elimination is the rate-determining step in the cycle. The

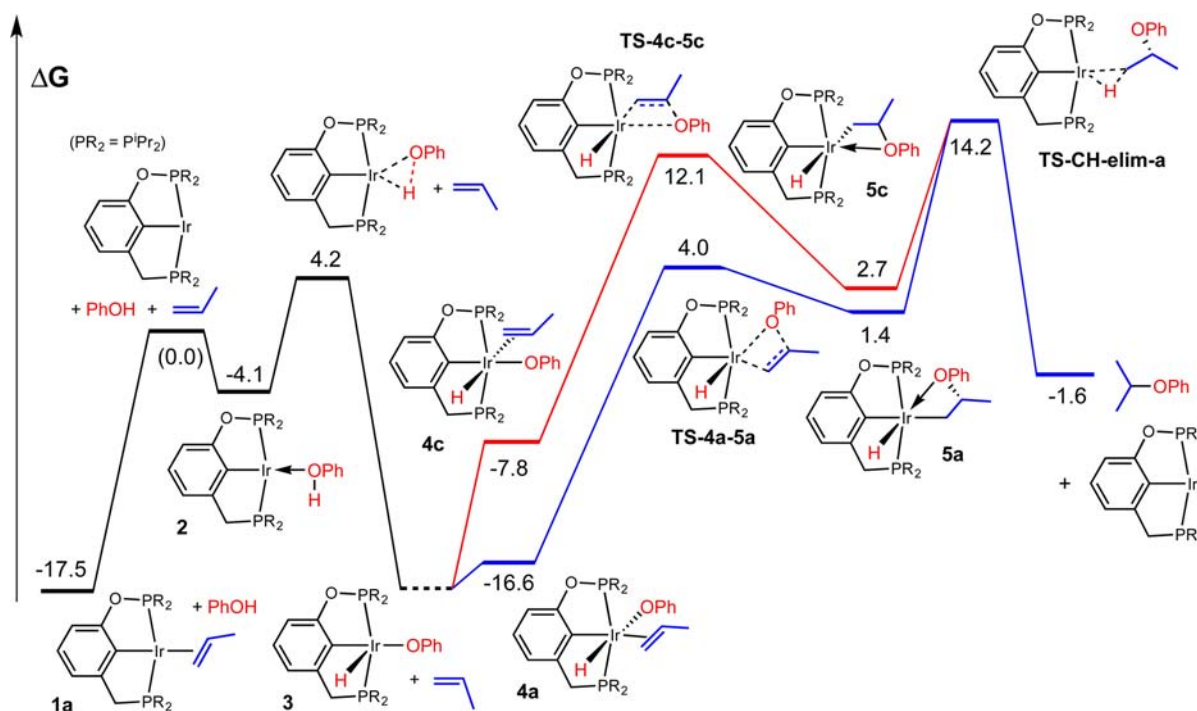


Figure 5. Free energy diagram (M06-L; values of ΔG in kcal/mol) for the proposed 1,2-Ir-O addition pathway for hydrophenoxylation of propene by $(i\text{Pr})\text{PCOPIr}$ to give *i*-PrOAr proceeding via “olefin-trans” (blue) and “olefin-cis” (red) pathways.

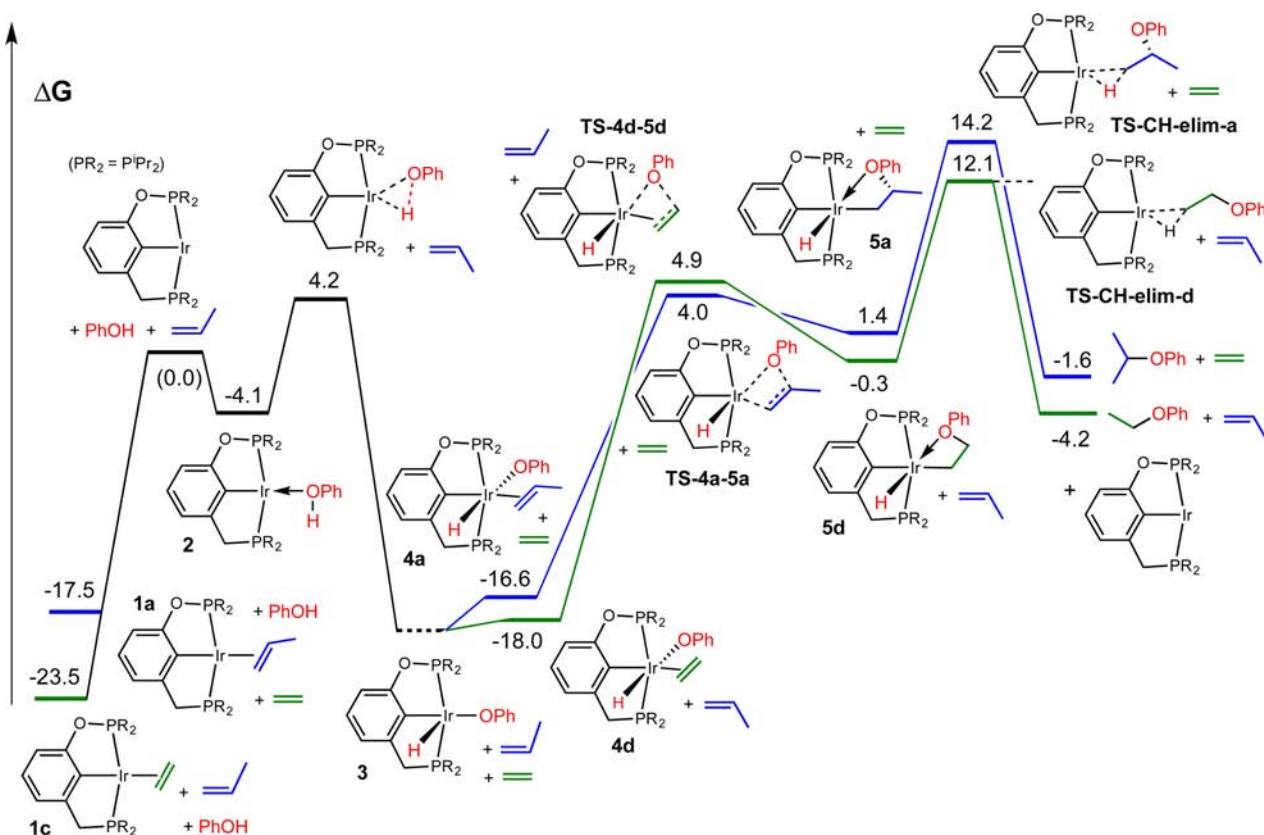


Figure 6. Free energy diagram (values in kcal/mol) for proposed pathway for hydrophenoxylation of ethylene (green lines) and propene (blue lines) by $(i\text{Pr})\text{PCOPIr}$. From a common resting state (as in a competition experiment) the barrier to the reaction of ethylene is lower, but in individual experiments, the overall barrier is lower for the reaction of propene.

calculations are in excellent agreement with experimental results, including the absolute rate and the selectivities for formation of *i*-PrOAr vs *n*-PrOAr (very high) and for dehydroaryloxylation of *i*-

PrOAr vs *n*-PrOAr (ca. 6-fold). Calculations using the M06 functional lead to essentially the same predictions, including the rate-determining nature of C–H elimination. However, whereas

the use of M06-L leads to barrier heights for C–H elimination that are much higher than for insertion (by 10.2 and 3.5 kcal/mol for 1,2-addition and 2,1-addition, respectively), the differences are much less pronounced using M06 (3.5 and 0.7 kcal/mol for 1,2-addition and 2,1 addition, respectively; see Tables S4 and S5 and Figure S4, Supporting Information). Thus, while DFT calculations obtained using either functional indicate that C–H elimination is rate determining for hydroaryloxylation (and C–H addition rate determining for dehydroaryloxylation), future studies to test this important conclusion seem warranted.

It should be noted that two geometrically distinct variants of either the 1,2- or 2,1-Ir–O addition pathways have been calculated. For each pathway there is the variant in which the olefin is initially coordinated trans to the PCP aryl of (ⁱPrPCOP)Ir(OPh)H (shown in Figure 3), and another in which olefin coordinates cis to the PCP aryl, while the phenoxy group is coordinated trans (shown in Figure 5 for 1,2-addition leading to *i*-PrOPh). The olefin-trans variant has a lower energy TS for insertion of olefin into the Ir–O bond in for both 1,2- and 2,1-additions. Each variant gives rise to a different isomer of (ⁱPrPCOP)Ir(phenoxypropyl)(H) upon Ir–O addition (5a vs 5c in the case of the 1,2-addition shown in Figure 5). In both cases the olefin-trans insertion TS is of higher energy than the olefin-cis TS (TS-4c-5c vs TS-4a-5a in the case of 1,2-addition). However, the intermediates resulting from Ir–O addition can probably interchange readily (the barrier to decoordination of the phenoxy group, as noted above, is only 7 kcal/mol). Thus even if the olefin-cis insertion were more facile than the olefin-trans pathway, since the insertion step is not rate determining the distinction between these pathways would not necessarily be significant.

Finally, Figure 6 illustrates the results of calculations for the addition of PhOH to ethylene proceeding via the mechanism of Figure 2b, along with the calculated values for the addition to propene in the presence of ethylene, thereby modeling the competition experiment of eq 4. The overall barrier for PhOH addition to ethylene (which is not affected by the presence of propene) is calculated to be 35.6 kcal/mol (the difference between the free energy of TS-CH-elim-d and the free energy of (ⁱPrPCOP)Ir(ethene) (1c)). The overall barrier for hydroaryloxylation of propene, *in the presence of ethylene* (which results in an ethylene-bound resting state), is calculated to be 37.7 kcal/mol (the free energy of TS-CH-elim-a minus the free energy of the resting state ethene complex 1c) as compared with 31.7 kcal/mol above the propene-bound resting state. Thus, these calculations successfully capture both the greater reactivity of ethylene in competition experiments *and* the greater reactivity of propene in independent runs, providing additional support for the proposed mechanism of Figure 2b. Interestingly, the TS for ethene insertion TS-4d-5d is slightly higher than that for propene insertion, TS-4a-5a. If that is in fact the case (although the small difference of 0.9 kcal/mol is arguably not meaningful), and if insertion into the Ir–O bond, not C–H elimination, were rate-determining, then the competition experiment of eq 4 would have yielded more *i*-PrOAr than EtOAr, in contrast with the experimental result.

CONCLUSIONS

We report iridium pincer complexes that catalyze olefin hydroaryloxylation with simple olefins and phenols. These catalysts do not operate via a “hidden Brønsted acid” mechanism, common to previously reported precatalysts for this reaction, as their high selectivity for O- vs C-alkylation and the preference for

addition to less substituted olefins make clear. DFT calculations are strongly supportive of a mechanism proceeding via insertion of olefin into the iridium–aryloxy Ir–O bond. A very high degree of regioselectivity is observed. DFT calculations indicate that this is determined by the energy of the respective TS's for C–H bond elimination; this derives in part from the same factors that control selectivity for C–H bond addition.

The nature of the sterically congested and geometrically well-defined pincer–metal unit, and the formation of secondary alkyl ethers, suggest an entry into the development of olefin hydroaryloxylation catalysis that may display unusual selectivity or enantioselectivity. More generally, the discovery of these well-defined nonacid catalysts suggests the possibility of catalytic intermolecular O–H addition across multiple bonds with a scope broader than that for phenols and simple olefins. Finally, we find that the catalysts are also effective for the reverse, C–O bond cleavage reaction, dehydroaryloxylation. Further research efforts in these contexts are underway.

ASSOCIATED CONTENT

Supporting Information

Text, figures, and tables giving experimental details and procedures, including synthesis of (ⁱPrPCOP)IrH₄, characterization of (ⁱPrPCOP)Ir(H)(OPh), and characterization of (ⁱPrPCOP)Ir(η^2 -propene), computational details, and molecular energies and geometries. This material is available free of charge via the Internet at <http://pubs.acs.org>.

AUTHOR INFORMATION

Corresponding Authors

kroghjes@rutgers.edu.
alan.goldman@rutgers.edu.

Notes

The authors declare no competing financial interest.

ACKNOWLEDGMENTS

This work was carried out under the auspices of National Science Foundation Grant CHE No. 1112456 and the Extreme Science and Engineering Discovery Environment (XSEDE), which is supported by National Science Foundation Grant No. OCI-1053575. M.C.H. thanks the NSF IGERT program (Renewable and Sustainable Fuel Solutions for the 21st Century) for a Graduate Training Fellowship. B.L. thanks the Rutgers–Jilin exchange program for funding.

REFERENCES

- (1) Hartwig, J. F. In *Organotransition Metal Chemistry*; University Science Books: Sausalito, CA, 2010; pp 667–699.
- (2) Yadav, J. S.; Antony, A.; Rao, T. S.; Subba Reddy, B. V. *J. Organomet. Chem.* **2011**, *696*, 16–36.
- (3) Ananikov, V. P.; Beletskaya, I. P. In *Hydrofunctionalization*; Ananikov, V. P., Tanaka, M., Eds.; Springer: Berlin, Heidelberg: 2013; Vol. 43, pp 1–19.
- (4) Muller, T. E.; Hultsch, K. C.; Yus, M.; Foubelo, F.; Tada, M. *Chem. Rev.* **2008**, *108*, 3795–3892.
- (5) Julian, L. D.; Hartwig, J. F. *J. Am. Chem. Soc.* **2010**, *132*, 13813–13822.
- (6) Julian, L. D. *Topics in Heterocyclic Chemistry*, Springer: Berlin, Heidelberg: 2013; pp 1–47.
- (7) For examples of lanthanide catalyzed intramolecular O–H addition to multiple bonds see: (a) Seo, S.; Yu, X.; Marks, T. J. *J. Am. Chem. Soc.* **2008**, *131*, 263–276. (b) Dzudza, A.; Marks, T. J. *Org. Lett.* **2009**, *11*, 1523–1526. (c) Dzudza, A.; Marks, T. J. *Chem. Eur. J.* **2010**, *16*, 3403–3422.

- (8) Fiege, H.; Voges, H.-W.; Hamamoto, T.; Umemura, S.; Iwata, T.; Miki, H.; Fujita, Y.; Buysch, H.-J.; Garbe, D.; Paulus, W. In *Ullmann's Encyclopedia of Industrial Chemistry*; Wiley-VCH: Weinheim, Germany, 2000.
- (9) Williamson, A. *Philos. Mag.* **1850**, *37*, 350–356.
- (10) Sowa, F. J.; Hinton, H. D.; Nieuwland, J. A. *J. Am. Chem. Soc.* **1932**, *54*, 3694–3698.
- (11) Yang, C.-G.; He, C. *J. Am. Chem. Soc.* **2005**, *127*, 6966–6967.
- (12) Rosenfeld, D. C.; Shekhar, S.; Takemiya, A.; Utsunomiya, M.; Hartwig, J. F. *Org. Lett.* **2006**, *8*, 4179–4182.
- (13) Li, Z.; Zhang, J.; Brouwer, C.; Yang, C.-G.; Reich, N. W.; He, C. *Org. Lett.* **2006**, *8*, 4175–4178.
- (14) Hintermann, L. In *C-X Bond Formation*; Vigalok, A., Ed.; Springer: Berlin, Heidelberg: 2010; Vol. 31, pp 123–155.
- (15) Dang, T. T.; Boeck, F.; Hintermann, L. *J. Org. Chem.* **2011**, *76*, 9353–9361.
- (16) Yamamoto, H.; Futatsugi, K. *Angew. Chem., Int. Ed.* **2005**, *44*, 1924–1942.
- (17) After this paper was submitted for publication, a report by Sevov and Hartwig on a Segphos–iridium-catalyzed olefin hydroaryloxylation appeared: Sevov, C. S.; Hartwig, J. F. *J. Am. Chem. Soc.* **2013**, *135*, 9303–9306.
- (18) Some of this work has been presented preliminarily: Haibach, M. C.; Li, B.; Wang, D. Y.; Guan, C.; Krogh-Jespersen, K.; Goldman, A. S. *Abstracts of Papers*; 245th ACS National Meeting & Exposition, New Orleans, LA, United States, April 7–11, **2013**; American Chemical Society: Washington, DC, **2013**; INOR-130.
- (19) Choi, J.; Choliy, Y.; Zhang, X.; Emge, T. J.; Krogh-Jespersen, K.; Goldman, A. S. *J. Am. Chem. Soc.* **2009**, *131*, 15627–15629.
- (20) Kundu, S.; Choi, J.; Wang, D. Y.; Choliy, Y.; Emge, T. J.; Krogh-Jespersen, K.; Goldman, A. S. *J. Am. Chem. Soc.* **2013**, *135*, 5127–5143.
- (21) See the Supporting Information for details.
- (22) Kundu, S.; Choliy, Y.; Zhuo, G.; Ahuja, R.; Emge, T. J.; Warmuth, R.; Brookhart, M.; Krogh-Jespersen, K.; Goldman, A. S. *Organometallics* **2009**, *28*, 5432–5444.
- (23) Zhu, K.; Achord, P. D.; Zhang, X.; Krogh-Jespersen, K.; Goldman, A. S. *J. Am. Chem. Soc.* **2004**, *126*, 13044–13053.
- (24) Ahuja, R.; Punji, B.; Findlater, M.; Supplee, C.; Schinski, W.; Brookhart, M.; Goldman, A. S. *Nat. Chem.* **2011**, *3*, 167–171.
- (25) Choi, J.; MacArthur, A. H. R.; Brookhart, M.; Goldman, A. S. *Chem. Rev.* **2011**, *111*, 1761–1779.
- (26) Haibach, M. C.; Kundu, S.; Brookhart, M.; Goldman, A. S. *Acc. Chem. Res.* **2012**, *45*, 947–958.
- (27) Pincer iridium dihydrides and tetrahydrides are well-known to undergo dehydrogenation by olefin and are therefore presumed to act simply as precursors of the corresponding (pincer)Ir fragment. Likewise, the ethylene adducts and the hydrido chlorides in the presence of strong base are known precursors of the same fragment. (a) Gupta, M.; Hagen, C.; Kaska, W. C.; Cramer, R. E.; Jensen, C. M. *J. Am. Chem. Soc.* **1997**, *119*, 840–841. (b) Renkema, K. B.; Kissin, Y. V.; Goldman, A. S. *J. Am. Chem. Soc.* **2003**, *125*, 7770–7771. (c) Göttker-Schnetmann, I.; White, P.; Brookhart, M. *J. Am. Chem. Soc.* **2004**, *126*, 1804–1811.
- (28) $(\text{Ir}^{\text{PCOP}})\text{IrH}_4$ was generated from the reported $(\text{Ir}^{\text{PCOP}})\text{Ir}(\text{C}_2\text{H}_4)$ complex and H_2 at room temperature. See the Supporting Information for experimental details and spectral data.
- (29) Dehydroalkoxylation, catalyzed by lanthanide triflates and thermodynamically driven by hydrogenation of the olefin product catalyzed by Pd nanoparticles (at 110 °C in the case of acyclic ethers), was recently reported by Marks and co-workers: Atesin, A. C.; Ray, N. A.; Stair, P. C.; Marks, T. J. *J. Am. Chem. Soc.* **2012**, *134*, 14682–14685.
- (30) Afeefy, H. Y.; Liebman, J. F.; Stein, S. E. Neutral Thermochemical Data. In *NIST Chemistry WebBook*; Linstrom, P. J., Mallard, W. G., Eds.; National Institute of Standards and Technology, Gaithersburg, MD, NIST Standard Reference Database Number 69, 20899, <http://webbook.nist.gov> (retrieved February 11, 2013).
- (31) Conversion from a mixture of products to exclusively $(\text{Ir}^{\text{PCOP}})\text{Ir}(\eta^2\text{-propene})$ is observed upon raising the temperature from ambient to 120 °C. It seems safe to assume that at 150 °C, the temperature of most of our experimental runs, the major species is still predominantly the same propene complex. Unfortunately, however, the temperature limits of our NMR spectrometers did not allow observation at this temperature. (Note that when the temperature is taken back down to ambient between intervals of heating at 150 °C, the original mixture is again observed, which, on warming to 120 °C in the NMR spectrometer, again yields exclusively $(\text{Ir}^{\text{PCOP}})\text{Ir}(\eta^2\text{-propene})$.)
- (32) Schwartz, J.; Labinger, J. A. *Angew. Chem., Int. Ed.* **1976**, *15*, 333–340.
- (33) Reger, D. L.; Culbertson, E. C. *Inorg. Chem.* **1977**, *16*, 3104–3107.
- (34) Some excellent lead references to organometallic C–H addition, with particular emphasis on selectivity: (a) Bennett, J. L.; Vaid, T. P.; Wolczanski, P. T. *Inorg. Chim. Acta* **1998**, *270* (1–2), 414–423. (b) Wick, D. D.; Jones, W. D. *Organometallics* **1999**, *18*, 495–505. (c) Asbury, J. B.; Hang, K.; Yeston, J. S.; Cordaro, J. G.; Bergman, R. G.; Lian, T. *J. Am. Chem. Soc.* **2000**, *122*, 12870–12871 and refs 4–11 therein. (d) Vetter, A. J.; Flaschenriem, C.; Jones, W. D. *J. Am. Chem. Soc.* **2005**, *127*, 12315–12322. (e) Balcells, D.; Clot, E.; Eisenstein, O. *Chem. Rev.* **2010**, *110*, 749–823.
- (35) Hartwig, J. F. In *Organotransition Metal Chemistry*; University Science Books: Sausalito, CA, 2010; pp 85–146.
- (36) Bryndza, H. E. *Organometallics* **1985**, *4*, 406–8.
- (37) Woerpel, K. A.; Bergman, R. G. *J. Am. Chem. Soc.* **1993**, *115*, 7888–7889.
- (38) Zhao, P.; Incarvito, C. D.; Hartwig, J. F. *J. Am. Chem. Soc.* **2006**, *128*, 9642–9643.
- (39) Tye, J. W.; Hartwig, J. F. *J. Am. Chem. Soc.* **2009**, *131*, 14703–14712.
- (40) Hartwig, J. F. *Nature* **2008**, *455*, 314–322.